

# Mott-Limited Thermopower of Pascal Electron Liquid Phases at the LaAlO<sub>3</sub>/SrTiO<sub>3</sub> Interface

Puqing Jiang, Yuhe Tang, Hyungwoo Lee, Jung-Woo Lee, Kitae Eom, Chang-Beom Eom, Heng Ban, Patrick Irvin, and Jeremy Levy\*

The thermoelectric properties of quasi-1D electron waveguides at the LaAlO $_3$ / SrTiO $_3$  interface at millikelvin temperatures are investigated. A highly enhanced and oscillating thermopower is found for these electron waveguides, with values exceeding 100  $\mu$ V K $^{-1}$  at 0.1 K in the electron-depletion regime. The Mott relation, which governs the band-term thermopower of noninteracting electrons, agrees well with the experimental findings in and around regimes where strongly attractive electron–electron interactions lead to a previously reported Pascal series of conductance explained by bound states of n=2,3,4,... electrons. These results pave the way for quantized thermal transport studies of emergent electron liquid phases in which transport is governed by quasiparticles with charges that are integer multiples or fractions of an electron.

#### 1. Introduction

The heterointerface between the complex oxides LaAlO<sub>3</sub> and SrTiO<sub>3</sub> (LAO/STO) provides a highly versatile platform to study electron correlations in low dimensions. A rich variety of electronically tunable properties have been observed in experiments that probe the behavior in two spatial dimensions, including superconductivity,<sup>[1,2]</sup> magnetism,<sup>[3]</sup> and tunable spin–orbit interactions.<sup>[4,5]</sup> Many unusual aspects of the transport in 2D appear to originate from naturally forming quasi-1D ferroelastic domain boundaries.<sup>[6,7]</sup> This behavior includes highly anisotropic magnetoresistance,<sup>[8,9]</sup> enhanced conductance along ferroelastic domain boundaries,<sup>[7]</sup> and quantum oscillations, whose Luttinger count disagrees sharply with Hall effect estimates of electron density. The importance of quasi-1D transport

P. Jiang, Y. Tang, P. Irvin, J. Levy
Department of Physics and Astronomy
University of Pittsburgh
Pittsburgh, PA 15260, USA
E-mail: jlevy@pitt.edu
H. Lee, J.-W. Lee, K. Eom, C.-B. Eom
Department of Materials Science and Engineering
University of Wisconsin-Madison
Madison, WI 33706, USA
H. Ban
Department of Mechanical Engineering and Materials Science
University of Pittsburgh
Pittsburgh, PA 15260, USA

The ORCID identification number(s) for the author(s) of this article can be found under https://doi.org/10.1002/pssb.202200612.

DOI: 10.1002/pssb.202200612

at the LAO/STO interface has been increasingly realized due to the deployment of various spatially resolved probes, including scanning SQUID microscopy, [7] scanning single-electron transistor microscopy, [10] and scanning force microscopy coupled with transport. [11]

Artificially created 1D electronic nanostructures have proven useful in teasing out the physics that is due to 2D versus 1D behavior. Using conductive atomic force microscope (c-AFM) lithography, LAO/STO heterostructures that are on the verge of an insulator-to-metal transition<sup>[12]</sup> can be made locally conductive by charging the surface (with protons)<sup>[13,14]</sup> at room temperature. This form of

modulation doping tetragonally distorts the conductive regions, "seeding" the formation of *z*-oriented ferroelastic domains at low temperatures. The resulting conductive nanostructures exhibit superconductivity, [11] electron pairing outside the superconducting phase, [15] ballistic quantized electron transport, [16] and other exotic phases in 1D such as a Pascal series of conductance  $(1,3,6,10,15,\dots)\cdot\frac{e^2}{h}$ , where e is the electron charge and h is the Planck constant. [17] Further nanoscale engineering of these electron waveguides leads to experimentally observed fractional conductance plateaus, which may be signatures of electron fractionalization.

Thermal transport experiments can provide unique and often complementary insights into correlated nanoelectronic phases. Thermopower measurements performed on 2D devices at the LAO/STO interface reported highly enhanced thermopower in the strongly depleted charge density regime, which was attributed to the phonon drag contribution, suggesting tight carrier confinement at the interface and the existence of a localized Anderson tail. Thermal transport techniques offer opportunities for obtaining further insight into the full phase diagram of these rich 1D systems.

#### 2. Experimental Section

Here, we describe thermopower measurements of electron waveguides that show ballistic transport and also exhibit signatures of a Pascal series of conductance steps associated with strong attractive electron—electron interactions. The electron waveguides were fabricated at the LAO/STO interface using c-AFM lithography. With 3.4 unit cells of LAO (quantified by in situ RHEED

15213951, 0, Downloaded from https://onlinelibrary.wiley.com/doi/10.1002/pssb.202200612 by University Of Pittsburgh University Library System, Wiley Online Library on [23.03/2023]. See the Terms and Conditions (https://onlinelibrary.wiley.com/term

conditions) on Wiley Online Library for rules of use; OA articles are governed by the applicable Creative Commons License

oscillations) grown on the TiO2-terminated STO substrate, the LAO/STO interface was initially insulating and could be rendered conductive using c-AFM lithography. [12] The interface was contacted electrically by depositing titanium and gold in lithographically defined areas that were etched below the LAO/STO interface, as illustrated in Figure 1b. Positive voltages applied between the c-AFM tip and the LAO/STO interface locally protonated the top LAO surface and accumulated conducting electrons in STO near the LAO/STO interface, thus defining the nanowire for electron conduction, while negative voltages locally restored the insulating phase, [12] as illustrated in Figure 1a,b. Two electron waveguide systems (Devices A and B) were sketched and tested independently; both of them consisted of the main channel of a nominal width  $w = 10 \,\mathrm{nm}$  (as quantified by erasure experiments<sup>[19]</sup>) and a total length of  $L_c = 1.2 \,\mu\text{m}$ , contacted by five terminal leads and one-side gate. The main channel contained two narrow barriers (with nominal width  $L_{\rm B}=10{\rm nm}$ ) that were separated by a distance of  $L_{\rm s}=0.6\,\mu m$ , as illustrated in Figure 1c. The side gate supplied a controlled voltage  $V_{\rm sg}$  that tuned the chemical potential  $\mu$  of the electron waveguide and thus the number of accessible quantum channels. Note that the two barriers with appropriate widths were essential to make the chemical potential of the electron waveguide tunable by the side-gate voltage, which would otherwise be impossible if there was only one or none of the barriers or if the barriers were either too wide or too narrow.

The relationship between  $V_{\rm sg}$  and  $\mu$ , governed by the so-called lever-arm ratio  $\alpha \equiv \frac{d\mu}{dV_{sg}}$ , was determined as  $\alpha =$  $8.0 \pm 0.2 \, \mu eV \, mV^{-1} \,$  for our Device A and  $6.3 \pm 0.2 \, \mu eV \, mV^{-1}$ for Device B through the analysis of nonequilibrium conductance. Novel properties, such as electron pairing without superconductivity, [15] tunable electron–electron interactions, [20] and Shubnikov-de Haas-like quantum oscillations, [21] have previously been revealed by studying quantum transport in similarly designed nanostructures.

The four-terminal electrical conductance G of the electron waveguide was first measured at temperature  $T = 80 \,\mathrm{mK}$  as a function of  $V_{sg}$  and  $\mu$ , in magnetic fields ranging from -9 to 9 T. Specifically, as illustrated in Figure 1c, a sinusoidal source voltage of  $V_s \sin(\omega t)$  with  $V_s = 100 \,\mu\text{V}$  and  $\frac{\omega}{2\pi} = 3.156 \,\text{Hz}$  was supplied on terminal 1 with terminal 2, acting as the drain, was grounded; the amplitudes of both the alternating current on terminal 2 ( $I_2$ ) and the voltage difference between terminals 3 and 4 ( $V_{34}$ ) at the same frequency  $\omega$  were measured using a lock-in amplifier. The conductance of the electron waveguide was determined as  $G = \frac{dI}{dV} = \frac{I_2}{V_{34}}$ . Quantized conductance steps were observed, with the conductance increasing with chemical potential by steps of roughly an integer multiple of the unit conductance  $G_0 = \frac{e^2}{h}$ . The observed conduction plateaus can be explained by Landauer quantization, for which the total conductance *G* depends on the number of available quantum channels,  $G = \left(\frac{e^2}{h}\right) \sum_i T_i(\mu)$ , where each energy sub-band available at the chemical potential  $\mu$  contributes one quantum of the conductance  $\frac{e^2}{h}$  with transmission probability  $T_i(\mu)$ . [22] The sub-band dispersion of the LAO/STO electron waveguide can be revealed by examining the transconductance  $\frac{\mathrm{d}G}{\mathrm{d}\mu}$  as a function of  $\mu$  and external magnetic field B, which is shown in Figure 2b,d. The transconductance peaks (bright areas) mark the boundaries where new sub-bands become available, and the sub-bands were separated by regions of dark areas  $(\frac{dG}{du} \rightarrow 0)$ , where the conductance was highly quantized. Some more interesting features of the band structures of the LAO/STO electron waveguide were also manifested from the transconductance. For example, several branches were sometimes locked together and then spread apart again, as shown in Figure 2b,d. At some special values of the magnetic field (such as  $B = \pm 3.5 \,\mathrm{T}$  for Device A and  $\pm 6 \,\mathrm{T}$  for Device B), multiple locked sub-bands contributed to the total conductance together, resulting in conductance steps roughly

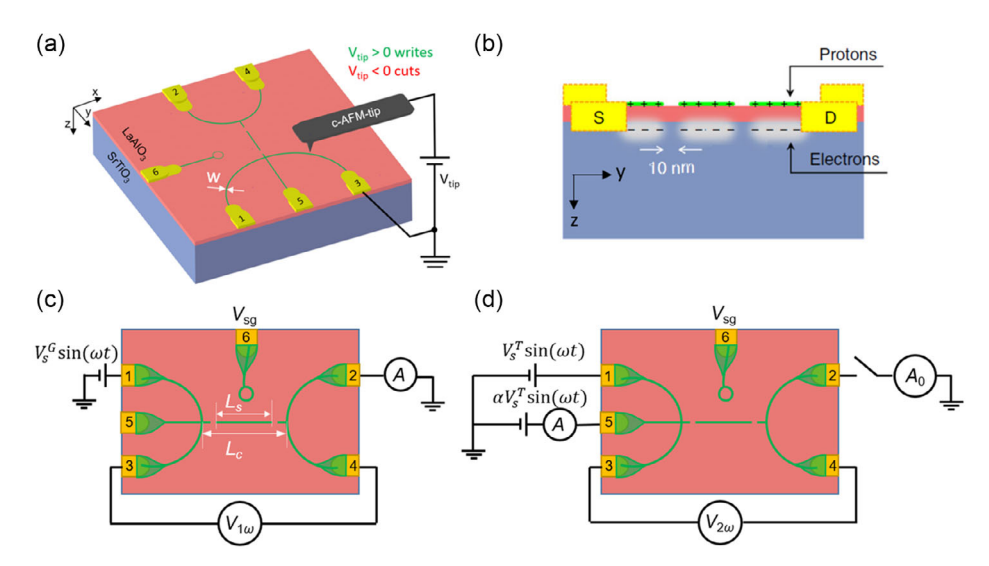
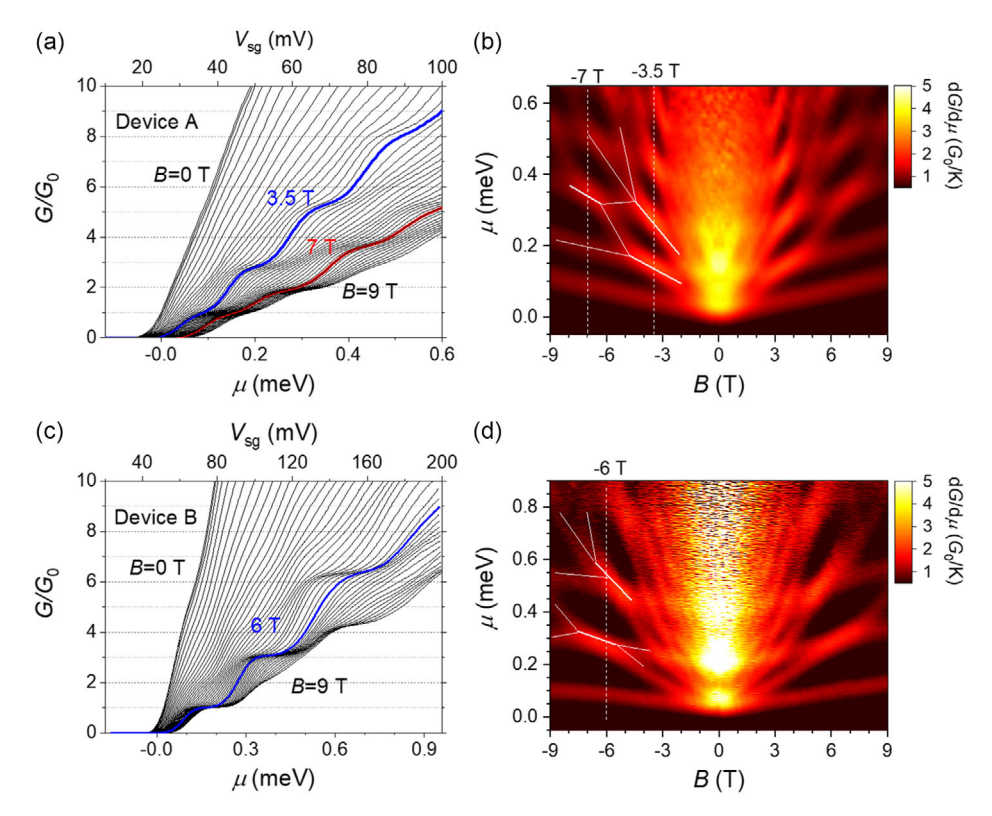


Figure 1. a) Schematic diagram of the four-terminal electron waveguide at the interface of LaAlO<sub>3</sub>/SrTiO<sub>3</sub> (LAO/STO) heterostructure created using c-AFM lithography. b) A side view of the sample showing the c-AFM-sketched quantum nanowire located at the interface of the LAO/STO heterostructure. c,d) Experimental design for the four-terminal conductance and thermopower measurement, respectively.

.5213951, 0, Downloaded from https://onlinelibrary

.wiley.com/doi/10.1002/pssb.202200612 by University Of Pittsburgh University Library System, Wiley Online Library on [23/03/2023]. See the Terms and Conditions

ditions) on Wiley Online Library for rules of use; OA articles are governed by the applicable Creative Commons



**Figure 2.** a,c) Zero-bias conductance of the quantum nanowires (Device A and B) as a function of chemical potential  $\mu$  and magnetic field B in the range 0–9 T at T=80 mK. b,d) Transconductance map  $\frac{dG}{d\mu}$  as a function of chemical potential  $\mu$  and magnetic field B at T=80 mK showing the band structure of electrons in the c-AFM-sketched LAO/STO quantum nanowires.

following the sequence of  $(1, 3, 6, 10, \dots) \cdot \frac{e^2}{h}$ . This behavior was previously reported as the Pascal phase and was explained by introducing attractive electron–electron interactions with bound states of  $n = 2, 3, 4, \dots$  electrons within the waveguide. [17]

Generally, the thermopower S was decomposed into two contributions, the electronic term  $S_{\rm e}$  and the phonon drag term  $S_{\rm ph}$  that was generated by the coupling of electrons with diffused phonons. The phonon drag contribution should be negligible in the temperature range of 0.1–0.4 K since the majority of the phonons (with  $\nu > \frac{10kT}{L} = 0.5\,\mathrm{THz}$  at 0.4 K) was frozen out at such low temperatures. [23] In linear response, the electronic term  $S_{\rm e}$  was given by the Mott relation [24,25] as

$$S_{\rm e} = \lim_{\Delta T \to 0} \frac{V_{\rm th}}{\Delta T} = -\frac{\pi^2}{3e} k_{\rm B}^2 T \frac{d}{d\mu} \ln G \tag{1}$$

where  $\Delta T = T_{\rm e} - T_{\rm l}$  is the temperature difference that generates the thermovoltage  $V_{\rm th}$ . The Mott relation states that the thermovoltage  $V_{\rm th}$  should be linearly proportional to the energy derivative of logarithmic conductance  $\frac{{\rm d}(\ln G)}{d\nu}$ .

To check whether the assumption of frozen-out phonons is valid and whether the Mott relation holds for LAO/STO electron waveguides, we compared the measured  $V_{\rm th}$  and  $\frac{d(\ln G)}{d\mu}$  in the same plot. Details of the measurement technique are described in Section S2, Supporting Information. **Figure 3** shows an example of Device A at the same temperature of 0.1 K and two

different magnetic fields of B = 0.5 (Figure 3a) and 3.5 T (Figure 3b), and another example of Device B at the same magnetic field of 6T and two different temperatures of 0.1T (Figure 3c) and 0.4 K (Figure 3d). We found that the measured  $V_{
m th}$  values compared very well with  $rac{{
m d}(\ln G)}{{
m d}u}$  in the conductive regime with  $G > 0.1 \frac{e^2}{h}$  irrespective of the device, the magnetic field, or the temperature. In the electron-depletion regime with  $G < 0.1 \frac{e^2}{h}$ , the number of electrons that could pass through the waveguide channel kept dropping with decreasing chemical potential; therefore, the magnitude of the measured thermovoltage  $V_{\mathrm{th}}$  dropped to zero though the value of  $\frac{\mathrm{d}(\ln G)}{\mathrm{d}\mu}$  kept increasing with reducing  $\mu$ . In the conductive regime, as the temperature increased, features attributable to the sub-band structure governing the electrical conductance G,  $\frac{\mathrm{d}G}{\mathrm{d}\mu}$ , and  $\frac{\mathrm{d}(\ln G)}{\mathrm{d}\mu}$  were thermally broadened. The measured thermovoltage  $V_{\mathrm{th}}$  also showed muted oscillatory features but still compared very well with  $\frac{d(\ln G)}{du}$ . The thermovoltage as a function of the side-gate voltage reached a local maximum every time the conductance changed from one plateau to the next and had a valley corresponding to each plateau of the conductance. Similar features were also observed on quantum point contacts, [26-29] where the thermopower as a function of gate voltage also had a peak every time the conductance plateau changed from one sub-band to the next.

The excellent agreement between  $V_{\rm th}$  and  $\frac{{\rm d}(\ln G)}{{\rm d}\mu}$  confirmed the validity of the Mott relation (Equation (1)) and allowed us to



15213951, 0, Downloaded from https://onlinelibrary.wiley.com/doi/10.1002/pssb.202200612 by University Of Pittsburgh University Library System, Wiley Online Library on [23/03/2021]. See the Terms and Conditions

onditions) on Wiley Online Library for rules of use; OA articles are governed by the applicable Creative Commons

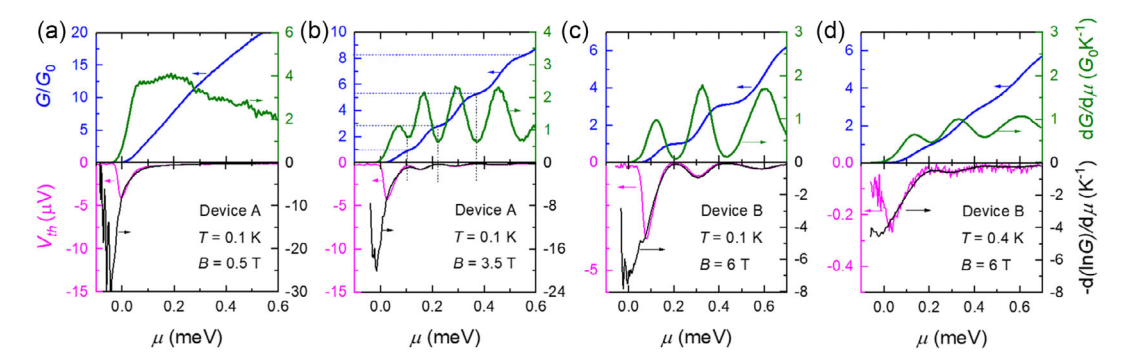


Figure 3. Thermopower voltage measurement. Top panels: Four-terminal conductance G and transconductance  $\frac{dG}{d\mu}$  as a function of chemical potential  $\mu$ . Bottom panels:  $V_{th}$  and  $\frac{d(\ln G)}{du}$ . (a) and (b) are taken from Device A at the same temperature of 0.1 K and different magnetic fields of 0.5 and 3.5 T, respectively. (c) and (d) Device B at the same magnetic field of 6 T and different temperatures of 0.1 and 0.4 K, respectively.

compute the gate-dependent temperature difference between the two sides of the electron waveguide

$$T_{\rm e} - T_{\rm l} = \sqrt{\frac{T_{\rm l}^2}{4} + \frac{1}{(-\frac{\pi^2}{2e}k_{\rm R}^2)} \frac{V_{\rm th}}{\frac{\rm d}{\rm d} \ln G}} - \frac{T_{\rm l}}{2}$$
 (2)

Figure 4a shows the corresponding electron temperatures calculated using Equation (2). We noted that the calculated electron temperatures in the conducting regime were not constant but rather oscillating with the chemical potential, especially at higher magnetic fields, which could be attributed to the sub-band shift with the magnetic field and the change of the number of conducting channels in the electron waveguide with the chemical potential. We also noticed that the calculated temperature difference reduced to zero as the electron waveguide was tuned to the insulating state, which, however, was not realistic, as a temperature difference should still exist even when the electron waveguide was insulating. This apparent disagreement could be explained by a space-charge effect proposed by Mahan, [30,31] who stated that the thermal voltage, instead of being  $V_{\rm th} = -S\Delta T$ , should read as  $V_{th} = -S\Delta T f$ , where f is the dielectric screening function and approaches zero as the electron density approaches zero (being insulating). This regime is also discussed by Brovman et al.[32] within the context of germanium/silicon nanowires. The measured thermal voltage being zero does not necessarily

require the Seebeck coefficient S and/or the temperature difference  $\Delta T$  to vanish. The temperature difference in the insulating regime (see also Figure S3, Supporting Information) was ignored here since we only focused on the conducting regime.

#### 3. Discussion

With the temperature difference determined, the Seebeck coefficient of the electron waveguide can be calculated from Equation (1), with the results plotted in Figure 4b. The negative sign of S confirms the electrons as energy carriers. The magnitude of the Seebeck coefficient S (the thermopower) increases dramatically as the electron waveguide is tuned to the electron depletion regime with G below  $0.1\frac{e^2}{h}$ , reaching as high as  $200 \,\mu\text{V K}^{-1}$  at only  $T = 0.1 \,\text{K}$ . Applied magnetic fields do not have a significant effect on the thermopower S.

The Mott relation also predicts that the thermopower *S* should be linearly proportional to the temperature. To test if this is true for our electron waveguide, we measure the thermopower of Device B in a magnetic field of B = 6T at different temperatures ranging from 100 to 400 mK and plot it as a function of normalized electrical conductance  $\frac{G}{G_0}$ , as shown in Figure 5a. We find that overall, the thermopower increases with temperature, although the scaling with temperature deviates from the

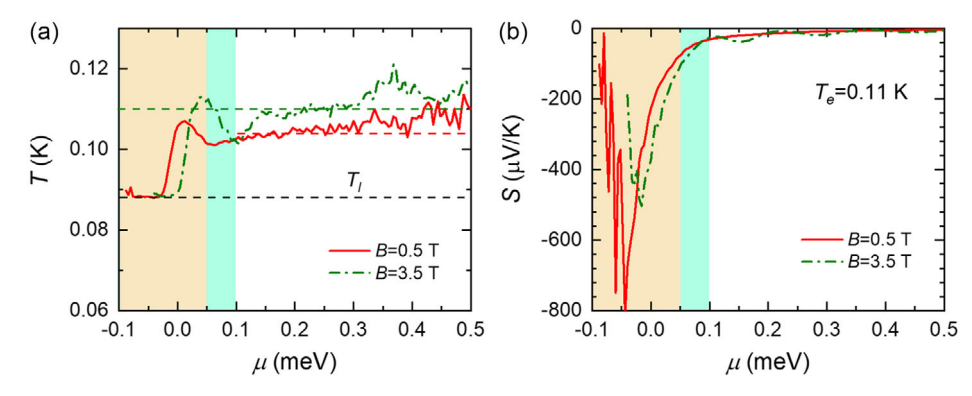


Figure 4. Derived a) electron temperature Te and b) Seebeck coefficients S of the electron waveguide (Device A) as a function of chemical potential for different magnetic fields of B = 0.5 and 3.5 T. The shadowed regions represent the electron depletion regimes with  $G < 0.1\frac{e^2}{h}$ .



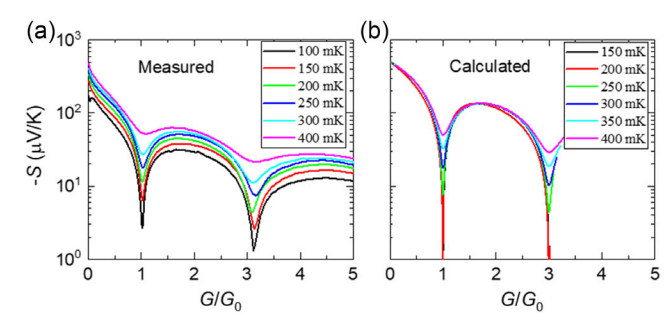


Figure 5. a) Measured thermopower of Device B in a magnetic field of B = 6 T at different lattice temperatures of 100–400 mK, plotted as a function of normalized electrical conductance  $\frac{C}{G_0}$ . b) Calculated thermopower according to the Mott relation (Equation (1)), based on the Fermi-Dirac distribution of carriers and Landauer conductance quantization.

straightforward linear-T dependence implied by the Mott formula. The thermopower has local minima (shown as dips in the plot) when the conductance reaches plateaus  $(G/G_0 = 1, 3, ...)$ , and these dips are smeared out as the temperature increases, leading to different temperature dependencies of the thermopower. The reason for these substantial deviations near conductance plateaus originates from the implicit temperature dependence inherent to the temperature-dependent Fermi function. Figure 5b shows the calculated thermopower based on Equation (1) and conductance given by the Landauer formula with sub-band energy minima and degeneracies that match Device B. The scaling of the thermopower with T for both the experiment and the model is sublinear with the temperature at  $G = 2G_0$ , a fact that could be accounted for by phonon-related thermopower contributions.

Lunde and Flensberg analyzed the validity of the Mott formula for quantum point contacts, [33] and the oscillatory dependence they calculate agrees well with our experimental findings. Strictly speaking, the Mott relation is derived based on the assumption of a noninteracting, degenerate electron gas. However, the electron gas in 1D-confined systems, which is a Luttinger liquid, is inevitably interacting. As discussed earlier, evidence shows that electrons strongly interact at LAO/STO interfaces.<sup>[15]</sup> Notably, the Pascal conductance sequence in some magnetic fields shown in Figure 2 indicates electron pairs in the electron waveguides outside the superconducting regime.<sup>[17]</sup>

## 4. Summary and Conclusion

In summary, the field-effect electrical transport and thermoelectric properties of quasi-1D electron waveguides at the LAO/STO interface are investigated at temperatures of 100-400 mK. These electron waveguides exhibit a highly enhanced and oscillating thermopower as a function of the side-gate voltage, which is well described by the Mott relation at a given fixed temperature, despite the evidence of strong electron-electron interactions in our electron waveguides outside the superconducting regime. These results demonstrate the capability to study electronic structures of nanowires at LAO/STO with thermal transport technique. Due to the fascinating electronic phases LAO/STO nanowires exhibit, this work can further lead to understanding quantized thermal conductance and other exotic electronic phases in LAO/STO systems.

## **Supporting Information**

Supporting Information is available from the Wiley Online Library or from the author.

# Acknowledgements

P.J. and Y.T. contributed equally to this work. The authors acknowledge Philip Kim for helpful feedback. J.L. acknowledges financial support from ONR N00014-15-1-2847, NSF PHY-1913034 and DMR-2225888. This research was funded by the Gordon and Betty Moore Foundation's EPiQS Initiative, grant GBMF9065, to Chang-Beom Eom.

### **Conflict of Interest**

The authors declare no conflict of interest.

# **Data Availability Statement**

The data that support the findings of this study are available from the corresponding author upon reasonable request.

## **Keywords**

complex oxide heterostructures, electron waveguides, thermopower, quantum transport, quasi-1D transport

> Received: December 28, 2022 Revised: February 27, 2023 Published online:

15213951, 0, Downloaded from https://onlinelibrary.wiley.com/doi/10.1002/pssb.202200612 by University Of Pittsburgh University Library System, Wiley Online Library on [23.03/2023]. See the Terms and Conditions (https://onlinelibrary.wiley.com/term

and-conditions) on Wiley Online Library for rules of use; OA articles are governed by the applicable Creative Commons

- [1] N. Reyren, S. Thiel, A. D. Caviglia, L. F. Kourkoutis, G. Hammerl, C. Richter, C. W. Schneider, T. Kopp, A.-S. Rüetschi, D. Jaccard, M. Gabay, D. A. Muller, J.-M. Triscone, J. Mannhart, Science 2007, 317, 1196.
- [2] A. D. Caviglia, S. Gariglio, N. Reyren, D. Jaccard, T. Schneider, M. Gabay, S. Thiel, G. Hammerl, J. Mannhart, J. M. Triscone, Nature 2008, 456, 624.
- [3] A. Brinkman, M. Huijben, M. van Zalk, J. Huijben, U. Zeitler, J. C. Maan, W. G. van der Wiel, G. Rijnders, D. H. A. Blank, H. Hilgenkamp, Nat. Mater. 2007, 6, 493.
- [4] A. D. Caviglia, M. Gabay, S. Gariglio, N. Reyren, C. Cancellieri, J. M. Triscone, Phys. Rev. Lett. 2010, 104, 126803.
- [5] M. Ben Shalom, M. Sachs, D. Rakhmilevitch, A. Palevski, Y. Dagan, Phys. Rev. Lett. 2010, 104, 126802.
- [6] H. Noad, E. M. Spanton, K. C. Nowack, H. Inoue, M. Kim, T. A. Merz, C. Bell, Y. Hikita, R. Xu, W. Liu, A. Vailionis, H. Y. Hwang, K. A. Moler, Phys. Rev. B 2016, 94, 174516.
- [7] B. Kalisky, E. M. Spanton, H. Noad, J. R. Kirtley, K. C. Nowack, C. Bell, H. K. Sato, M. Hosoda, Y. Xie, Y. Hikita, C. Woltmann, G. Pfanzelt, R. Jany, C. Richter, H. Y. Hwang, J. Mannhart, K. A. Moler, Nat. Mater. 2013. 12. 1091.
- [8] P. K. Rout, I. Agireen, E. Maniv, M. Goldstein, Y. Dagan, Phys. Rev. B **2017**, 95, 241107.

15213951, 0, Downloaded from https://onlinelibrary.wiley.com/doi/10.1002/pssb.202200612 by University Of Pittsburgh University Library System, Wiley Online Library on [23.03/2023]. See the Terms

conditions) on Wiley Online Library for rules of use; OA

- [9] H. J. H. Ma, J. Zhou, M. Yang, Y. Liu, S. W. Zeng, W. X. Zhou, L. C. Zhang, T. Venkatesan, Y. P. Feng, Ariando, *Phys. Rev. B* 2017, 95, 155314.
- [10] M. Honig, J. A. Sulpizio, J. Drori, A. Joshua, E. Zeldov, S. Ilani, Nat. Mater. 2013, 12, 1112.
- [11] Y. Y. Pai, H. Lee, J. W. Lee, A. Annadi, G. Cheng, S. Lu, M. Tomczyk, M. Huang, C. B. Eom, P. Irvin, J. Levy, *Phys. Rev. Lett.* **2018**, *120*, 147001
- [12] S. Thiel, G. Hammerl, A. Schmehl, C. W. Schneider, J. Mannhart, Science 2006. 313, 1942.
- [13] F. Bi, D. F. Bogorin, C. Cen, C. W. Bark, J.-W. Park, C.-B. Eom, J. Levy, Appl. Phys. Lett. 2010, 97, 173110.
- [14] K. A. Brown, S. He, D. J. Eichelsdoerfer, M. Huang, I. Levy, H. Lee, S. Ryu, P. Irvin, J. Mendez-Arroyo, C. B. Eom, C. A. Mirkin, J. Levy, Nat. Commun. 2016, 7, 10681.
- [15] G. Cheng, M. Tomczyk, S. Lu, J. P. Veazey, M. Huang, P. Irvin, S. Ryu, H. Lee, C. B. Eom, C. S. Hellberg, J. Levy, *Nature* 2015, 521, 196.
- [16] A. Annadi, G. Cheng, H. Lee, J. W. Lee, S. Lu, A. Tylan-Tyler, M. Briggeman, M. Tomczyk, M. Huang, D. Pekker, C. B. Eom, P. Irvin, J. Levy, *Nano Lett.* 2018, 18, 4473.
- [17] M. Briggeman, M. Tomczyk, B. Tian, H. Lee, J.-W. Lee, Y. He, A. Tylan-Tyler, M. Huang, C.-B. Eom, D. Pekker, R. S. K. Mong, P. Irvin, J. Levy, Science 2020, 367, 769.
- [18] I. Pallecchi, F. Telesio, D. Li, A. Fete, S. Gariglio, J. M. Triscone, A. Filippetti, P. Delugas, V. Fiorentini, D. Marre, *Nat. Commun.* 2015, 6, 6678.

- [19] C. Cen, S. Thiel, G. Hammerl, C. W. Schneider, K. E. Andersen, C. S. Hellberg, J. Mannhart, J. Levy, Nat. Mater. 2008, 7, 298.
- [20] G. Cheng, M. Tomczyk, A. B. Tacla, H. Lee, S. Lu, J. P. Veazey, M. Huang, P. Irvin, S. Ryu, C.-B. Eom, A. Daley, D. Pekker, J. Levy, Phys. Rev. X 2016, 6, 041042.
- [21] G. Cheng, A. Annadi, S. Lu, H. Lee, J. W. Lee, M. Huang, C. B. Eom, P. Irvin, J. Levy, *Phys. Rev. Lett.* **2018**, *120*, 076801.
- [22] S. Datta, Quantum Transport: Atom to Transistor, Cambridge University Press, Cambridge 2005.
- [23] J. M. Ziman, Electrons And Phonons: The Theory of Transport Phenomena in Solids, Clarendon Press, New York 1960.
- [24] M. Cutler, N. F. Mott, Phys. Rev. 1969, 181, 1336.
- [25] M. Jonson, G. D. Mahan, Phys. Rev. B 1980, 21, 4223.
- [26] C. R. Proetto, Phys. Rev. B 1991, 44, 9096.
- [27] A. S. Dzurak, C. G. Smith, L. Martin-Moreno, M. Pepper, D. A. Ritchie, G. A. C. Jones, D. G. Hasko, J. Phys.: Condens. Matter 1993, 5, 8055.
- [28] N. J. Appleyard, J. T. Nicholls, W. R. Tribe, M. Y. Simmons, M. Pepper, *Physica E* 2000, 6, 534.
- [29] A. Jouan, G. Singh, E. Lesne, D. C. Vaz, M. Bibes, A. Barthélémy, C. Ulysse, D. Stornaiuolo, M. Salluzzo, S. Hurand, J. Lesueur, C. Feuillet-Palma, N. Bergeal, *Nat. Electron.* 2020, 3, 201.
- [30] G. D. Mahan, J. Electron. Mater. 2015, 44, 431.
- [31] G. D. Mahan, J. Electron. Mater. 2016, 45, 1257.
- [32] Y. M. Brovman, J. P. Small, Y. Hu, Y. Fang, C. M. Lieber, P. Kim, J. Appl. Phys. 2016, 119, 234304.
- [33] A. M. Lunde, K. Flensberg, J. Phys.: Condens. Matter 2005, 17, 3879.